The biphasic force–velocity relationship in frog muscle fibres and its evaluation in terms of cross-bridge function

K. A. P. Edman, A. Månsson and C. Caputo

Department of Pharmacology, University of Lund, S-223 62 Lund, Sweden

1. The relationship between force and velocity of shortening was studied during fused tetani of single fibres isolated from the anterior tibialis muscle of *Rana temporaria* (1·5–3·3 °C; sarcomere length, 2·20 μm). Stiffness was measured as the change in force that occurred in response to a 4 kHz length oscillation of the fibre.

2. The results confirmed the existence of two distinct curvatures of the force–velocity relationship located on either side of a breakpoint in the high-force, low-velocity range. Reduction of the isometric force (P_0) to 83·4 ± 1·7% (mean ± S.E.M., $n = 5$) of the control value by dantrolene did not affect the relative shape of the force–velocity relationship. The breakpoint between the two curvatures was located at 75·9 ± 0·9% of P_0 and 11·4 ± 0·6% of maximum velocity of shortening (V_{max}) in control Ringer solution and at 75·6 ± 0·7% of P_0 and 12·2 ± 0·7% of V_{max} in the presence of dantrolene. These results provide evidence that the transition between the two curvatures of the force–velocity relationship is primarily related to the speed of shortening, not to the actual force within the fibre.

3. The instantaneous stiffness varied with the speed of shortening forming a biphasic relationship with a breakpoint near $0{\cdot}15\,V_{max}$ and $0{\cdot}8P_0$, respectively. The force/stiffness ratio (probably reflecting the average force per cross-bridge), increased with force during shortening. The increase of the force/stiffness ratio with force was less steep at forces exceeding $0{\cdot}8P_0$ than below this point.

4. A four-state cross-bridge model (described in the Appendix) was used to evaluate the experimental results. The model reproduces with great precision the characteristic features of the force–stiffness–velocity relationships recorded in intact muscle fibres.

The force–velocity relationship represents a fundamental property of the contractile system: the ability of muscle to adjust its active force to precisely match the load by varying the speed of shortening appropriately. Fenn & Marsh (1935) were the first to describe the inverse relationship between force and velocity of shortening in frog skeletal muscle. Hill (1938) later extended these studies and characterized the force–velocity relationship as a rectangular hyperbola. He further emphasized the usefulness of the force–velocity relationship as a relevant index of muscle activity. The force–velocity relationship has attracted much new interest in recent years as it has become clear that it contains relevant information concerning the cross-bridge mechanism of muscle contraction (Huxley, 1957; Eisenberg & Hill, 1978; Eisenberg, Hill & Chen, 1980; see also Edman, 1979 and Woledge, Curtin & Homsher, 1985).

Studies on isolated skeletal muscle fibres have shown that the force–velocity relationship is not a simple hyperbolic function as was originally thought, but that it contains two distinct curvatures located on either side of a breakpoint at 75–80% of the isometric force, P_0 (Edman, Mulieri & Scubon-Mulieri, 1976; Edman, 1988). The composite form of the force–velocity relationship can be fitted well by an extended version of Hill's (1938) hyperbolic equation (Edman, 1988), the latter function providing a useful tool for expressing the inter-relationship between the two curvatures. There is reason to believe that the biphasic shape of the force–velocity relationship represents the contractile behaviour at sarcomere level. This is indicated by the fact that the force–velocity relationship has the same biphasic shape when measurements are made from the whole fibre and from short segments along the same intact muscle fibre (Edman, 1988). The biphasic nature of the force–velocity relationship has also been demonstrated in skinned muscle fibres (K. A. P. Edman, unpublished observations; Lou & Sun, 1993). The existence of the high-force curvature has important implications for muscle function in that it promotes mechanical stability of the contractile system in situations where the muscle is heavily loaded (see Discussion).

In the present study the nature of the biphasic shape of the force–velocity relationship has been explored in isolated muscle fibres of the frog. Simultaneous measurements of force and stiffness have been performed to evaluate the number of attached cross-bridges in relation to the active force and speed of shortening as the fibre contracts under different loads. Experiments have also been performed with

the specific aim of investigating whether the transition between the two curvatures of the force–velocity relationship is primarily related to the speed of shortening or to the force produced by the fibre. This problem has been approached by varying the state of activation of the contractile system by dantrolene, an agent known to reduce the release of activator calcium from the sarcoplasmic reticulum (e.g. Van Winkle, 1976; Desmedt & Hainaut, 1977; Danko, Kim, Sreter & Ikemoto, 1985).

Some of the results have previously been reported in a preliminary form (Edman, 1993; Edman & Caputo, 1993). The present paper provides a full account of the study including the statistical evaluation of the experimental results. Furthermore, a four-state cross-bridge model has been employed to elucidate the nature of the biphasic force–stiffness–velocity relationships in striated muscle.

METHODS

Preparation and mounting

Single fibres were isolated from the anterior tibialis muscle of cold-adapted *Rana temporaria* as previously described (Edman, 1979). The frogs were killed by decapitation followed by destruction of the spinal cord. The fibres were mounted horizontally in a temperature-controlled chamber of methyl methacrylate (Perspex) between a force transducer and an electromagnetic puller. In some experiments the fibre was mounted between two pullers, one producing rapid, low-amplitude movements for stiffness measurements (Edman & Lou, 1990), the other performing larger movements for isovelocity recordings (Edman & Reggiani, 1984). The second puller was provided with a force transducer to which one end of the fibre was attached. The tendons were held by aluminium clips that were attached to the hooks of the force transducer and puller arm as previously described (Edman & Reggiani, 1984). The side parts of the aluminium clips were folded tightly around the hooks to prevent any change in position of the clip during the experiment. By carefully adjusting the angle at which the clip was attached to the steel hook, it was possible to almost completely eliminate any lateral, vertical and twisting movements of the fibre during contraction. A special arrangement had to be used for attaching the fibre to the fast puller used for stiffness measurements (Edman & Lou, 1990). In this case the tendon (without the aluminium clip) was tied to the free end of the puller arm. Two layers of sealing film (Parafilm) were wound tightly onto the outside of the tendon around the puller arm in order to ensure firm attachment of the tendon throughout the experiment.

Fibre length, cross-sectional area and sarcomere length were measured as described by Edman & Reggiani (1984). The experiments were carried out at a resting sarcomere length of 2·20 μm.

The saline used had the following composition (mM): NaCl, 115·5; KCl, 2·0; $CaCl_2$, 1·8; $Na_2HPO_4 + NaH_2PO_4$, 2·0; pH 7·0. The solution was pre-cooled and was perfused through the muscle chamber (volume, ~2·5 ml) at a rate of about 2 ml min^{-1}. The temperature ranged from 1·5 to 3·3 °C among the different experiments but was maintained constant to within $\pm$0·2 °C during any given experiment. Dantrolene sodium (Eaton Chemicals, Norwich, NY, USA) was dissolved in Ringer solution to a final concentration of 5–10 mg l^{-1} (15–30 μM).

Stimulation

A pair of platinum plate electrodes were placed symmetrically on either side of the muscle fibre approximately 2 mm from it. Rectangular current pulses of 0·2 ms duration were passed between the electrodes, the stimulus strength being approximately 15% above the threshold. A train of pulses of appropriate frequency (15–20 Hz) was used to produce a fused tetanus of 1 s at the sarcomere length considered.

Force transducer

The force transducer generally used was made from a semi-conductor strain-gauge element and had a resonant frequency of approximately 6 kHz (Edman & Reggiani, 1984). A modified version of this transducer, which was used for stiffness measurements, had a resonant frequency of 19 kHz when submerged in saline (for details, see Edman & Lou, 1990).

Measurement of fibre stiffness

Stiffness was measured as the change in force that occurred in response to a fast, low-amplitude length perturbation as previously described (Edman & Lou, 1990). A 4 kHz sinusoidal length oscillation was applied to one end of the fibre throughout the tetanus period. The amplitude of the length oscillation (peak to peak) corresponded to approximately 1·5 nm per half-sarcomere (h.s.). With the technique used it was possible to obtain on-line information of the magnitude of the length perturbation and of the resulting change in force (for further details see Edman & Lou, 1990). In these measurements the force transducer was mounted on the puller that produced large fibre movements (see above). Since this arrangement increased the noise level of the stiffness signal during load-clamp recording, isovelocity ramps were preferred in experiments where force, velocity of shortening and stiffness were recorded simultaneously.

Experiments were performed in which a fast release step was applied to one end of the fibre with simultaneous recording of the resulting length change of a marked segment (1·7 mm long) located in the middle of the fibre. The segment length measurement was carried out by means of the surface marker technique previously described (Edman & Reggiani, 1984; Edman & Lou, 1990). The length step, which had a rise time of 200 μs and an amplitude of 2–3 nm $h.s.^{-1}$ in three different experiments, was applied at various tension levels during the rising phase of a fused tetanus. Five to six releases were repeated at each level and a mean value of the segment length change was formed. The segment length change did not differ significantly at force levels greater than 40% of maximum tetanic force indicating that the error in the fibre stiffness measurement due to tendon compliance was negligible under these conditions.

Recording and measurement of responses

Force, stiffness, fibre length and segment length signals were recorded and measured using a Nicolet 4094B digital oscilloscope that was provided with a dual disk recorder (Nicolet, XF44). Measurements of force, stiffness and velocity of shortening were made approximately 10 ms after release at the lowest loads used. The measurements were performed successively later after release as the load was increased and the velocity of shortening was reduced. With the approach used all measurements in a series of force–stiffness–velocity recordings (carried out between $0{\cdot}4P_0$ and P_0, see Results) could be performed without appreciable variation in sarcomere length (estimated variation $< 0{\cdot}03$ μm). No correction for length-dependent differences in force (Edman & Reggiani, 1987) and stiffness (e.g. Bagni, Cecchi, Colomo & Poggesi, 1990) within a series of measurements were therefore made.

The force–velocity data were fitted by the biphasic equation previously described by Edman (1988):

$$V = \frac{(P_0^* - P)b}{P + a}\left(1 - \frac{1}{1 + \exp(-k_1(P - k_2 P_0))}\right), \quad (1)$$

in which V denotes the velocity of shortening and P is the load on the muscle fibre. The first term expresses the hyperbolic portion of the force–velocity curve below $0{\cdot}8P_0$ and has the designations originally given by Hill (1938). P_0^* is the isometric force predicted from this hyperbola and a and b are constants with dimensions of force and velocity, respectively. The second term within parentheses (referred to as the 'correction term'; Edman, 1988) reduces V in the high-force range to provide the distinct, upward-concave curvature at loads $> 0{\cdot}8P_0$. The constant k_1 in the correction term has the dimension of 1/force, whereas k_2 is dimensionless.

V_{max}, the speed of shortening at zero load, was estimated from Hill's (1938) hyperbolic equation fitted to data below $0{\cdot}8P_0$.

Statistics

Student's t test was used for determination of statistical significance. All statistics are given as means ± S.E.M.

RESULTS

Force–velocity relationship at different states of activation

Previous experiments (Edman, 1988) have shown that the force–velocity relationship of striated muscle has two distinct curvatures located on either side of a breakpoint near 80% of the measured P_0. At this point the speed of shortening is approximately 11% of V_{max}. The aim of the following experiments was to investigate whether the transition between the two curvatures is primarily related to the load on the fibre, or to the speed of shortening. The rationale of the experimental approach is as follows. If the change in curvature in the high-force range is a consequence of increasing the number of interacting cross-bridges above a critical value, the relative load at which the breakpoint appears should vary with the state of activation of the contractile system. A decrease in activation would thus be expected to shift the breakpoint between the two curvatures towards a higher relative load, and finally, when the state of activation has been reduced to 80% of P_0, the high-force curvature would disappear altogether. In order to test this possibility a series of experiments was performed in which the force–velocity relationship was determined before and after the state of activity of the muscle fibre was depressed by dantrolene.

A set of load-clamp recordings including one or more isometric tetani was first performed in ordinary Ringer solution using the technique previously described (Edman, 1988). The fibre was thereafter immersed in Ringer solution containing dantrolene (5–10 mg l^{-1}) and a new series of load-clamp recordings was carried out during the plateau phase of the tetanus. As is illustrated in Fig. 1, dantrolene reduced the rate of rise of force and also reduced the plateau tension during the isometric tetanus (P_0). In five complete experiments P_0 was reduced to 83·4 ± 1·7% ($P < 0{\cdot}001$) of the control value. The calculated value of V_{max} was reduced by dantrolene to 93·0 ± 2·2% ($P < 0{\cdot}05$) of the control in the same experiments. Results of load-clamp recordings from a representative experiment are shown in Fig. 2. The figure shows force–velocity data derived at 2·2 μm sarcomere length in ordinary Ringer solution (○) and in the presence of 10 mg l^{-1} dantrolene (●). As can be seen in Fig. 2*A*, dantrolene reduced P_0 to approximately 80% of the control and shifted the force–velocity relationship towards lower force values. The biphasic force–velocity equation (eqn (1)) has been fitted to the experimental data in Fig. 2*A* and can be seen to provide a very good fit over the entire range of loads in both test and control runs. The constant k_2 in this equation (see Methods), which determines the breakpoint of the force–velocity curve relative to P_0, was quite similar both in the presence and in the absence of dantrolene (see legend to Fig. 2).

In Fig. 2*B* the force–velocity relationships shown in Fig. 2*A* have been replotted after the data have been normalized with respect to P_0 in each set. The superimposed data confirm that the general shape of the force–velocity relationship was not markedly changed by dantrolene. The similarity in shape of the two force–velocity relationships is further illustrated in the semilogarithmic plots shown in Fig. 2*C*. Here, the two portions of the force–velocity relationship

Figure 1. Effects of dantrolene on the time course of isometric tetanus of frog single muscle fibre
Records from the same fibre in control Ringer solution (upper trace) and in the presence of 10 mg l^{-1} dantrolene (lower trace). Dantrolene decreases the rate of rise of force and reduces the total amplitude of the tetanus. Fibre length at 2·20 μm sarcomere length, 6·0 mm. Temperature, 3·2 °C.

Table 1. Effects of dantrolene (5–10 mg l^{-1}) on P_0 and breakpoint of force–velocity relationship

	Control Ringer	Dantrolene
P_0 (% of value recorded in control Ringer)	100	83·4 ± 1·7
Relative force at breakpoint (% of P_0 recorded in control Ringer and dantrolene, respectively)	75·9 ± 0·9	75·6 ± 0·7
Relative velocity at breakpoint (% of V_{max} recorded in control Ringer and dantrolene, respectively)	11·4 ± 0·6	12·2 ± 0·7

$n = 5$.

(located on either side of the breakpoint in the high-force range) have been fitted by regression lines. As can be seen, there is a good agreement between the corresponding regressions in the two sets of data. The breakpoint between the two phases of the force–velocity relationship was determined from the intersection of the regression lines at low–intermediate and high loads in the semilogarithmic plots. The results from five experiments, similar to those illustrated in Fig. 2, are summarized in Table 1. The calculated breakpoint was located at 75·9 ± 0·9% of P_0 and 11·4 ± 0·6% of V_{max} ($n = 5$) in control Ringer solution and at 75·6 ± 0·7% of P_0 and 12·2 ± 0·7% of V_{max} in the presence of dantrolene. Student's t test on paired observations showed that the co-ordinates for the breakpoint of the force–velocity relationship were not significantly different in the presence and absence of dantrolene ($P > 0·1$). Thus, these results clearly show that even after the force-producing capability of the fibre has been markedly reduced by dantrolene, the characteristic biphasic shape of the force–velocity relationship is maintained.

Force–stiffness–velocity relationships

As explained in the Methods, isovelocity ramps were preferred to load-clamp recordings in these experiments. When forces lower than 70–80% of P_0 were studied, the shortening ramp was provided with an initial rapid phase, the amplitude of which was adjusted appropriately so as to achieve a relatively quick drop in tension to the desired level. Following an initial transient phase after the onset of shortening, force and stiffness settled at a constant level that varied with the shortening speed (see Fig. 7 in Curtin & Edman, 1994). Only stiffness measurements derived at forces greater than *ca* 40% of P_0 are considered here, since, down to this tension level (see Methods), there was no detectable interference in the stiffness measurement from tendon compliance.

Figure 3*A* shows superimposed, simultaneous force–velocity (○) and stiffness–velocity (●) measurements from a single muscle fibre during tetanus. The stiffness–velocity relationship can be seen to have a biphasic shape with a pronounced

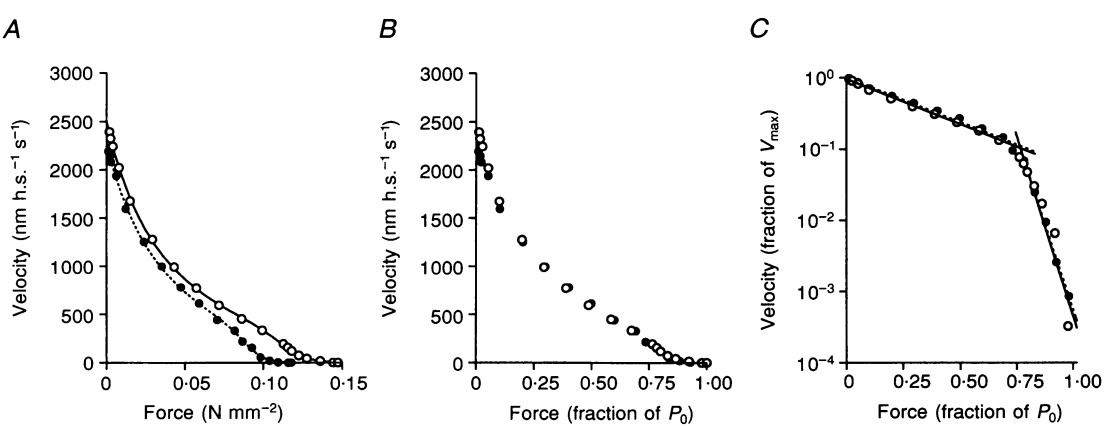

Figure 2. Influence of dantrolene on biphasic force–velocity relationship

○, control Ringer solution; ●, Ringer solution containing 10 mg l^{-1} dantrolene. *A*, force expressed in N mm^{-2}. *B*, force normalized to maximum tetanic force (P_0) in both test and control. *C*, semilogarithmic plots with force normalized to P_0 and velocity normalized to the calculated value of maximum speed of shortening, V_{max} in each set of data (see Methods). Data in *A* fitted by eqn (1) using the following numerical values for constants: control: $k_1 = 29P_0^{-1}$, $k_2 = 0·79$; dantrolene: $k_1 = 27P_0^{-1}$, $k_2 = 0·81$. The straight lines in *C* are linear regressions of velocity upon force on either side of the breakpoint of the force–velocity relationship. Continuous lines, control; dotted lines, dantrolene. Fibre length at 2·20 μm sarcomere length, 7·0 mm. Temperature, 1·5 °C.

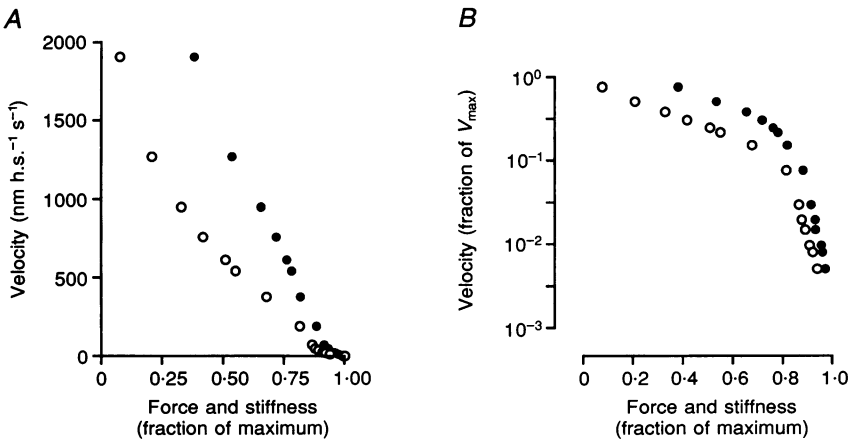

Figure 3. Force–velocity and stiffness–velocity relationships derived from simultaneous measurements in single muscle fibre

A, conventional plots (linear scales) with force and stiffness normalized to their maximum tetanic values. ○, force–velocity measurements; ●, stiffness–velocity measurements. *B*, a semilogarithmic plot of the data shown in *A*. Note the biphasic shape of both force–velocity and stiffness–velocity relationships. Fibre length at 2·20 μm sarcomere length, 7·1 mm. Temperature, 2·5 °C.

upward-concave curvature in the low-velocity range similar to that exhibited by the force–velocity relationship. The biphasic nature of the stiffness–velocity relationship is further demonstrated in Fig. 3*B* in which the data shown in Fig. 3*A* have been replotted in a semilogarithmic diagram. The transition between the two phases of the stiffness–velocity relationship was, in general, less distinct than the corresponding change of the force–velocity relationship. In seven experiments performed in this series the transition between the two phases of the stiffness–velocity relationship occurred at 0·1–0·2 V_{max} and 0·8–0·9 P_0.

The relationship between force and stiffness during shortening is illustrated by a representative experiment in Fig. 4*A*. For this analysis the force and stiffness values were collected at given velocities of shortening at loads varying between approximately 0·4 and 1·0 P_0. Figure 4*B* shows, for comparison, the relationship between force and stiffness during redevelopment of isometric force in the same muscle fibre. For the latter measurement the fibre was released during the tetanus plateau by a moderately fast ramp (amplitude, 35–45 nm h.s.$^{-1}$; duration, 3·0 ms) that led to a complete drop in tension followed by redevelopment of force.

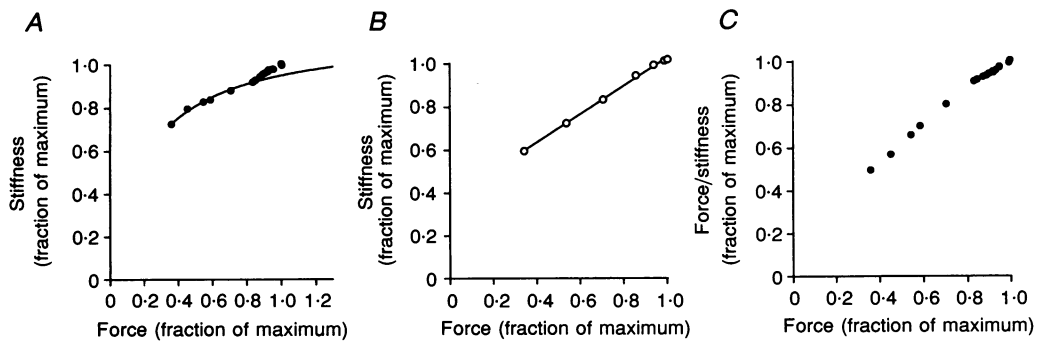

Figure 4. Force–stiffness relationships during loaded shortening and during isometric force development

Force and stiffness expressed as a fraction of maximum tetanic values. *A*, simultaneous measurements of force and stiffness during loaded shortening as described in text. The continuous line is a rectangular hyperbola fitted to data at forces $\leq 0{\cdot}8 P_0$. Note biphasic shape of the force–stiffness relationship during active shortening resulting in greater stiffness in the high-force range than predicted from measurements at intermediate forces. *B*, simultaneous measurements of force and stiffness during redevelopment of force in a tetanus. The continuous line is the linear regression of stiffness upon force. *C*, the ratio between force and stiffness, calculated from data in *A*, plotted against force. Note that the relationship between the force/stiffness ratio and force is less steep in the high-force range. Fibre length at 2·20 μm sarcomere length, 7·6 mm (*A* and *C*) and 7·1 mm (*B*). Temperature, 1·6 °C (*A* and *C*) and 2·5 °C (*B*).

The force–stiffness relationship measured during active shortening (Fig. 4*A*) can be seen to have two distinct portions with a point of transition near $0{\cdot}85P_0$. The data points between 0·4 and $0{\cdot}8P_0$ form a slightly downward-concave curvature and are fitted with a rectangular hyperbolic function. The stiffness values in the high-force range ($> 0{\cdot}85P_0$) can be seen to depart from this line. Thus, as the load was increased above $0{\cdot}85P_0$, the stiffness during shortening became successively higher than predicted from measurements at intermediate loads.

The biphasic shape of the force–stiffness relationship which was observed during shortening did not appear when measurements were performed during redevelopment of force in an isometric tetanus (Fig. 4*B*). In the latter case the force–stiffness relationship was steeper than that recorded during shortening and, most significantly, was lacking the high-force curvature displayed in Fig. 4*A*.

Results similar to those illustrated in Fig. 4*A* were obtained in altogether seven complete experiments. The difference between the predicted stiffness at P_0 (estimated from the hyperbola) and the stiffness actually measured at this point provides an index of the high-force deviation of the force–stiffness relationship during shortening. This difference amounted to $6{\cdot}5 \pm 0{\cdot}7\%$ ($P < 0{\cdot}001$) of the measured stiffness at P_0 in the seven fibres investigated.

The force/stiffness ratio presumably reflects the average force output per cross-bridge. As may be inferred from the force–stiffness relationships shown in Fig. 4*A* and *B*, the force/stiffness ratio increases with force during both shortening and isometric activity. This is further demonstrated in Fig. 4*C* for active shortening using the force–stiffness data shown in Fig. 4*A*. The relationship between the force/stiffness ratio and the load can be seen to have two distinct phases, with different slopes, on either side of the break-point near $0{\cdot}8P_0$. Beyond this point, corresponding to the high-force curvature of the force–velocity relationship, the increase of the force/stiffness ratio with force can be seen to be less steep than at intermediate forces.

Model simulation

A cross-bridge model including four different states, one dissociated and three attached states, was used to simulate the force–stiffness–velocity relationships presented above. A more detailed description of the model is given in the Appendix. The model is similar to the models previously advanced by Huxley & Simmons (1971) and Eisenberg *et al.* (1980) and has the following features (Fig. 5). During a complete working cycle a cross-bridge is assumed to go through three consecutive states of attachment, A_0, A_1 and A_2, each step leading to a progressively stronger binding to the actin unit and to further production of force by the bridge. Under isometric conditions, when the myofilament system is stationary, only the first two attachment states (A_0 and A_1) will be of importance due to the limited working range of the bridge. During shortening, on the other hand, the cross-bridge will pass over into the third and most strongly bound state (A_2). Finally, the bridge dissociates to become available for a new working cycle (A_3).

The cross-bridge model simulates the experimental results remarkably well as is illustrated in Fig. 6. The simulated data points displayed in Fig. 6*A* thus form a biphasic force–velocity relationship like that recorded in an intact muscle fibre exhibiting a smooth transition between the two curvatures near $0{\cdot}8P_0$ and $0{\cdot}1\,V_{max}$. Accordingly the simulated data can be fitted well with the biphasic force–velocity equation (Edman, 1988) using numerical values of the parameters k_1 and k_2 in this equation that are similar to those employed in frog muscle fibres ($k_1 \approx 30\ P_0^{-1}$, $k_2 \approx 0{\cdot}8$; Edman, 1988 and present paper). The simulation presented in Fig. 6*A* is based on the assumption that the rate constant ($k_{30}(x)$) for attachment to A_0 is independent of the speed of shortening of the fibre. A fairly high numerical value of $k_{30}(x)$ (maximum value 96 s^{-1}, see Appendix) is required in order to reproduce the relatively high velocities that exist at intermediate loads in intact fibres. However, a considerably lower maximum value of $k_{30}(x)$ (approximately 40 s^{-1}) is needed to correctly simulate the rising phase of an isometric tetanus at the temperature (1–3 °C) considered. In order to accommodate both these requirements in the model, k_{30} (here referred to as $k_{30}(x,v)$) has been assumed in the following analysis of force, velocity and stiffness to have a maximum numerical value of 96 s^{-1} for velocities of shortening ranging between V_{max} and $0{\cdot}14\,V_{max}$ (225 nm h.s.$^{-1}$ s^{-1}) and to decline below this point (see Appendix) to attain a value of 40 s^{-1} at $V = 0$. Also with these assumptions included in the model the predicted force–velocity relationship becomes virtually indistinguishable from a force–velocity curve of an intact fibre. This is illustrated in Fig. 6*B* which displays the simulated data in a standard force–velocity diagram and in Fig. 6*C* in which the same data are shown in a semilogarithmic plot.

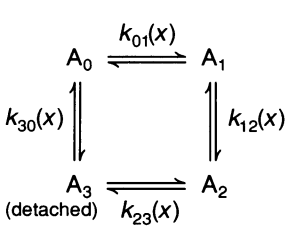

Figure 5. Kinetic scheme of cross-bridge model

Each state (A_0–A_3) has a characteristic strain dependence of its free energy (see Fig. 8) due to the presence of an elastic element in the cross-bridge. The rate constants for transitions between states are dependent on the relative position (x) between the cross-bridge and the actin site as shown in Fig. 9.

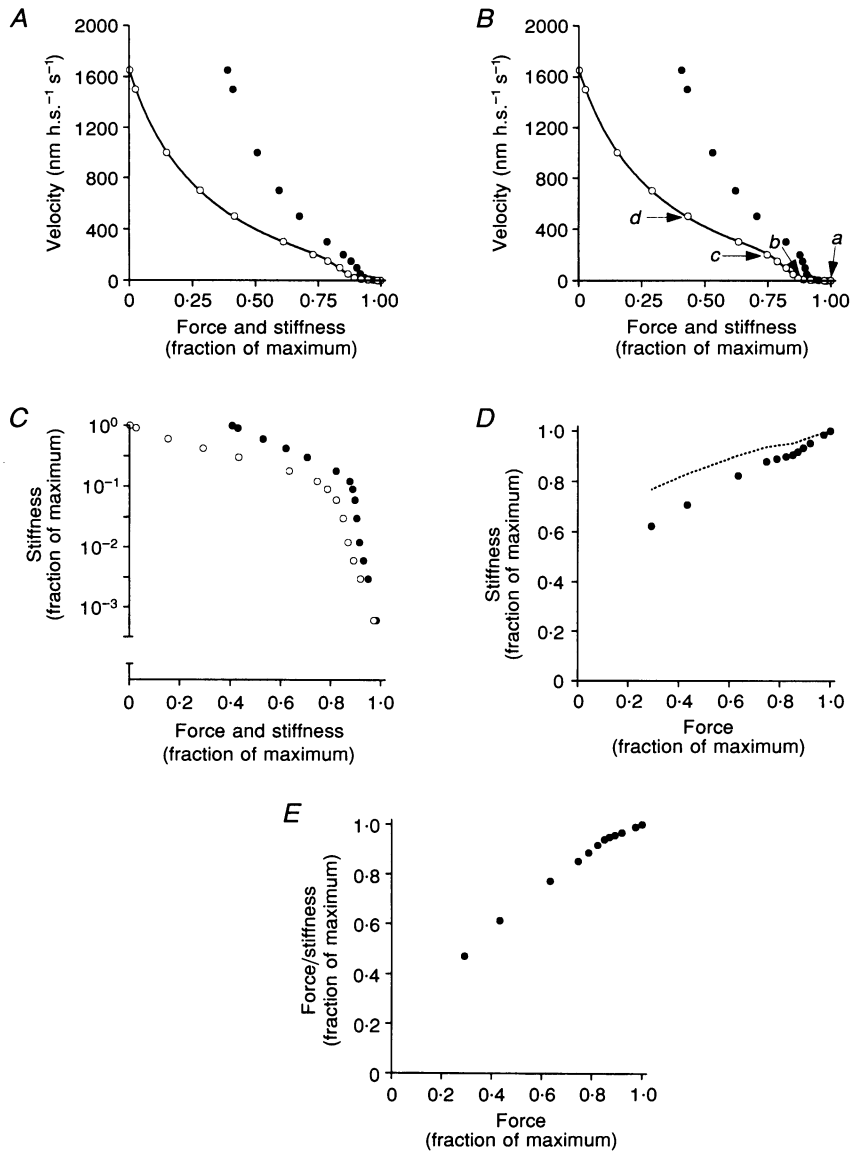

Figure 6. Model simulations of steady-state mechanical properties of frog muscle fibres during shortening

A, force–velocity (○) and stiffness–velocity (●) relationships simulated on the assumption that rate constant $k_{30}(x)$ in the model is independent of the velocity of shortening and has a maximum numerical value of 96 s^{-1}. The x dependence of this and other rate constants is shown in Fig. 9. The continuous line is eqn (1) fitted to simulated force–velocity data ($k_1 = 28P_0^{-1}$, $k_2 = 0{\cdot}83$). Force and stiffness expressed as a fraction of their maximum steady-state values. *B*, force–velocity (○) and stiffness–velocity (●) relationships simulated as in *A* but assuming that the rate constant $k_{30}(x,v)$ varies with the speed of shortening as described in text and in Fig. 9. The continuous line is eqn (1) fitted to simulated force–velocity data ($k_1 = 31P_0^{-1}$, $k_2 = 0{\cdot}82$). Arrows *a*–*d* indicate the corresponding data points for the cross-bridge distributions shown in Fig. 7. *C*, data shown in *B* replotted in a semilogarithmic diagram. *D*, force–stiffness relationship based on simulated force and stiffness values during loaded shortening. Data (●) collected at different velocities in diagram *B*. The dotted line shows, for comparison, the force–stiffness relationship during active shortening if it is assumed that the free portion of the thin filament forms a linear series elastic element. In this calculation the thin-filament compliance was assumed to be equal to that derived from the cross-bridges during the plateau of the isometric tetanus. *E*, the ratio between force and stiffness, calculated from the data points (●) in *D*, plotted against force.

The simulated stiffness–velocity relationship and the force–stiffness relationship during shortening are also found to agree well with measurements on intact muscle fibres as is illustrated in Fig. 6*A–D*. The calculated stiffness–velocity relationship thus forms a distinct curvature (upwards concave) in the low-velocity range. Further in similarity with the intact fibre the simulated force–stiffness relationship during isotonic shortening (Fig. 6*D*) can be seen to exhibit a biphasic shape with a breakpoint near $0{\cdot}85P_0$ (cf. Fig. 4*A*). As the load is raised beyond this point there is a steepening of the force–stiffness relationship resulting in higher stiffness values between $0{\cdot}85P_0$ and P_0 than predicted from data at intermediate loads. The model also reproduces the biphasic relationship between the force/stiffness ratio and force that was observed experimentally (Fig. 6*E*). Again the similarity with the corresponding observation in the intact fibre is striking (cf. Fig. 4*C*).

Figure 7 shows the proportion of cross-bridges in the different states of the model: during steady-state isometric contraction (*A*), during shortening at a very low speed (20 nm h.s.$^{-1}$ s^{-1}; *B*), during shortening at 200 nm h.s.$^{-1}$ s^{-1} (*C*) and during shortening at 500 nm h.s.$^{-1}$ s^{-1} corresponding to approximately one-third of V_{max} (*D*). The four conditions are indicated by arrows in Fig. 6*B*. Under isometric conditions (Fig. 7*A*) the bridges are almost exclusively attached to A_0 and A_1 since very few bridges are able to reach attachment state A_2 in this case. The flat portion of the force–velocity relationship in the high-force range (> approximately $0{\cdot}85P_0$) is accounted for in the model by a relatively large decrease in the number of cross-bridges in state A_0 as the fibre shortens at a low speed (Fig. 7*B*). Furthermore, the cross-bridges occupying A_0 during low-velocity shortening have a smaller mean extension than have bridges attached to A_0 under isometric conditions (cf. *A* and *B* in Fig. 7) resulting in a lower force output per bridge. Taken together these changes will cause a relatively large drop in force while the speed of shortening is only slightly increased. The steep portion of the force–velocity relationship between approximately $0{\cdot}85P_0$ and $0{\cdot}80P_0$ is attributable to an increased number of cross-bridges moving into attachment state A_2 as the speed of shortening is raised (Fig. 7*C*). This will partly compensate for the loss of bridges in state A_0, and force will therefore decline comparatively little as the speed of shortening increases within this range leading to an increased slope of the force–velocity relationship.

When the speed of shortening is raised above approximately 200 nm h.s.$^{-1}$ s^{-1}, which corresponds to about $0{\cdot}1\,V_{max}$, an increasing fraction of the bridges in state A_2 will assume negative x values in this way producing a braking force

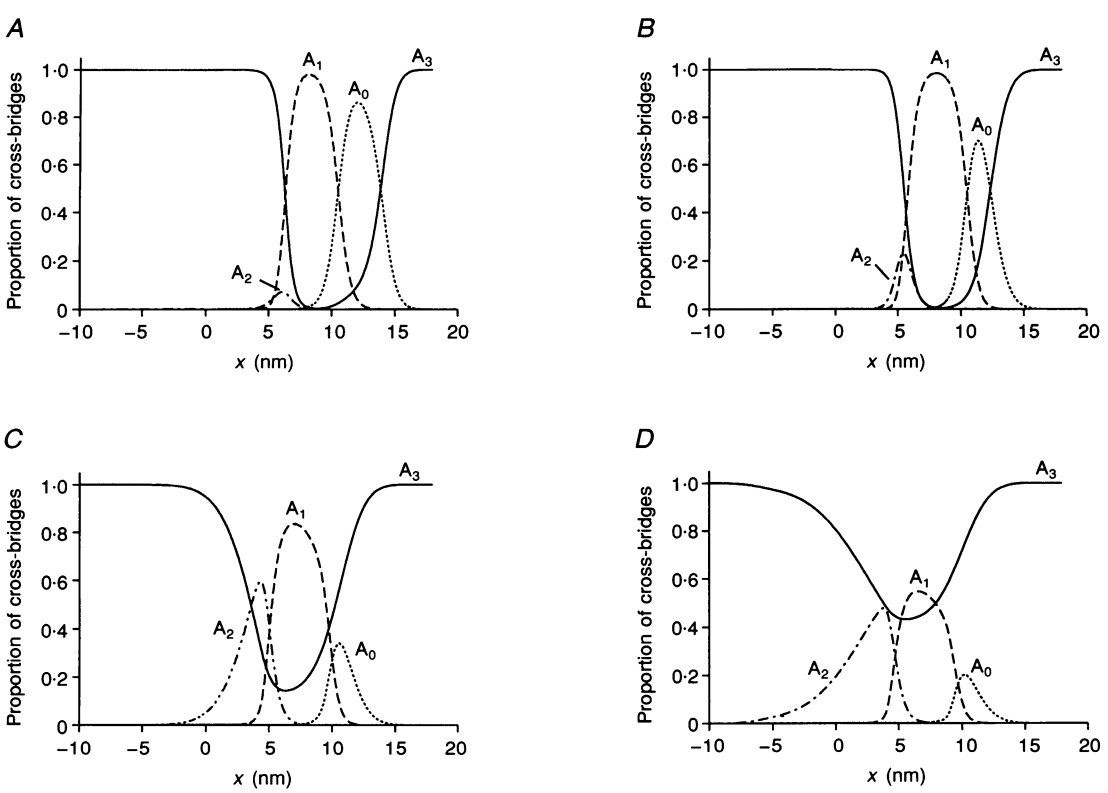

Figure 7. Proportion of cross-bridges in the various states (A_0–A_3) of the model given as a function of the distance (x) between cross-bridge and actin binding site

The cross-bridge distributions shown in *A–D* correspond to data points *a–d* in Fig. 6*B* and represent: *A*, steady-state isometric tension; *B*, steady shortening at 20 nm h.s.$^{-1}$ s^{-1}; *C*, steady shortening at 200 nm h.s.$^{-1}$ s^{-1}; *D*, steady shortening at 500 nm h.s.$^{-1}$ s^{-1}.

(Fig. 7*D*). Furthermore there will be a progressive reduction of the total number of attached bridges as the velocity increases above this point. These factors will both tend to reduce the slope of the force–velocity relationship resulting in a breakpoint of the force–velocity curve near $0{\cdot}8P_0$.

The present model, like most previous cross-bridge models, does not account for compliance of the thick and thin filaments. Recent evidence suggests, however, that the two filaments do have a finite stiffness that is comparable to that residing in the cross-bridges (Huxley, Stewart, Sosa & Irving, 1994; Kojima, Ishijima & Yanagida, 1994; Wakabayashi, Sugimoto, Tanaka, Ueno, Takezawa & Amemiya, 1994; Higuchi, Yanagida & Goldman, 1995). At the present time there is incomplete information concerning the nature of the filament elasticity, i.e. whether it is Hookean or not and whether it is equally distributed along the filaments or mainly involves the 'free' portions of the filaments outside the overlap area. In view of these uncertainties, involvement of filament compliance has been omitted in the present analysis. However, tests have been performed during the course of this study in which half of the instantaneous fibre compliance has been assumed to reside in the thin filaments as a series elastic element. The outcome of such tests has shown that introduction of series compliance in the model does not, in any fundamental way, affect the predicted mechanical behaviour during steady-state contractions, such as the predicted biphasic force–velocity relationship. The presence of series compliance will have the effect of making the fibre stiffness less sensitive to the speed of shortening, i.e. to changes in the number of attached bridges. This will result in a less steep force–stiffness relationship during shortening than in the absence of series elasticity (dotted line in Fig. 6*D*).

DISCUSSION

Experimental findings

The force–velocity relationship of frog skeletal muscle exhibits two distinct curvatures, both with an upward concavity, that are located on either side of a breakpoint at 76–78% of the isometric force (P_0). This characteristic form of the force–velocity relationship is demonstrable in both whole muscle fibres and discrete segments of intact fibres, and it probably represents the contractile behaviour at sarcomere level (Edman, 1988). The two portions of the force–velocity relationship are closely interrelated. A change of the main curvature is thus generally found to be associated with a similar change of the curvature in the high-force range. The entire force–velocity relationship can be fitted well with the biphasic equation previously described (Edman, 1988). In this equation the two constants k_1 and k_2 (eqn (1); see Methods) together define the interrelationship between the two portions of the force–velocity curve, k_1 expressing the degree of curvature in the low-velocity (high-force) range and k_2 determining the point of transition between the two portions of the force–velocity curve. In any given fibre similar numerical values of k_1 and k_2 are found to apply under a variety of experimental conditions such as altered temperature, tonicity and sarcomere length (Edman, 1988). There is evidence, however, that the two portions of the force–velocity relationship can be affected differentially. An example of such a dual action is provided by BDM (2,3-butanedione monoxime) which increases the curvature of the force–velocity relationship at low and intermediate loads but markedly reduces the curvature in the high-force range (Sun, Lou & Edman, 1995).

The present results show that the biphasic shape of the force–velocity relationship is well maintained even after reducing the tetanic force to about 80% of the control value by dantrolene. This substance is known to reduce the release of calcium from the sarcoplasmic reticulum (for references, see Introduction) and the decrease in force produced in this way may therefore be presumed to be mainly due to a reduced number of interacting cross-bridges. The fact that the relative shape of the force–velocity relationship remains unaffected after depressing the isometric force by dantrolene clearly demonstrates that the transition to the high-force curvature is not governed by the actual force within the fibre. The speed of shortening apparently is the principal factor that sets the point (approximately $0{\cdot}1\,V_{max}$) at which the force–velocity relationship changes its shape. This finding fully supports the idea that cross-bridges in striated muscle act as independent force generators under various loading conditions of the muscle. The cross-bridge model employed in this study is based on this assumption (see Appendix).

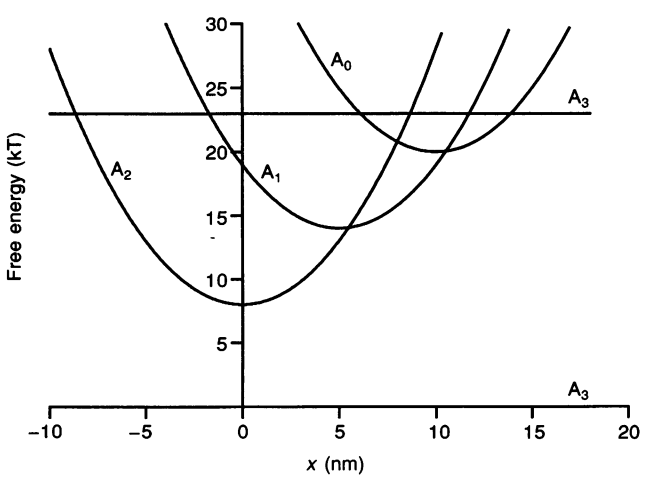

Figure 8. Gibbs free energy of cross-bridge states A_0–A_3 plotted as a function of the cross-bridge position relative to an actin binding site

The upper horizontal line and the abscissa represent, respectively, the free energy of the cross-bridges in state A_3 before and after hydrolysis of one molecule of ATP. The free energy available from hydrolysis of one molecule of ATP was taken to be 23 kT (Eisenberg *et al.* 1980).

With the approach used it was possible to monitor both force and stiffness as the fibre was released to shorten at different speeds during tetanus. The results show that the stiffness–velocity relationship is biphasic, like the force–velocity curve, with a breakpoint at approximately $0{\cdot}15\,V_{max}$. The force/stiffness ratio, which is generally thought to reflect the average force per cross-bridge, likewise undergoes a change when the speed of shortening is reduced below $0{\cdot}15\,V_{max}$ ($\sim 0{\cdot}8P_0$). The force/stiffness ratio measured during shortening increases steadily with force (Fig. 4*C*). However, as the load exceeds approximately $0{\cdot}8P_0$ the increase of the force/stiffness ratio is markedly reduced, suggesting that the force output per bridge is lower in the high-force range than expected from measurements at low and intermediate loads (Fig. 4*C*).

Model simulation

The force–velocity relationship was simulated by using a cross-bridge model the details of which are described in the Appendix. The model is based on the same general assumptions that were originally advanced by Huxley (1957) and Huxley & Simmons (1971) and further developed by Hill (1974), Eisenberg *et al.* (1980) and Piazzesi & Lombardi (1995). In accordance with these models the force during shortening is assumed in the present computations to be a function of the attachment rate constant of the cross-bridges, the distance traversed by the bridges during the working stroke and the rate constant of cross-bridge detachment. The latter rate constant determines how far the bridges may be brought into a region where they develop negative strain and resist fibre shortening. The detachment rate constant, therefore, is a major determinant (together with the size of the working stroke) of the maximum speed of shortening, V_{max}. In the present model, as in the models described by Huxley & Simmons (1971), Hill (1974), Eisenberg *et al.* (1980) and Piazzesi & Lombardi (1995), force generation is assumed to occur in several steps, each step leading to a tighter binding between actin and myosin and to a greater production of force.

Neither of the models referred to above account for the biphasic shape of the force–velocity relationship described in this paper and in earlier work (Edman, 1988, 1993; Sun *et al.* 1995). The present model, on the other hand, reproduces with remarkable precision the steady-state mechanical behaviour of intact muscle fibres during shortening. Both the experimental force–velocity relationship and the stiffness–velocity relationship are thus fitted exceedingly well. In addition (see Appendix), the model gives a faithful reproduction of the time course of the isometric tetanus and

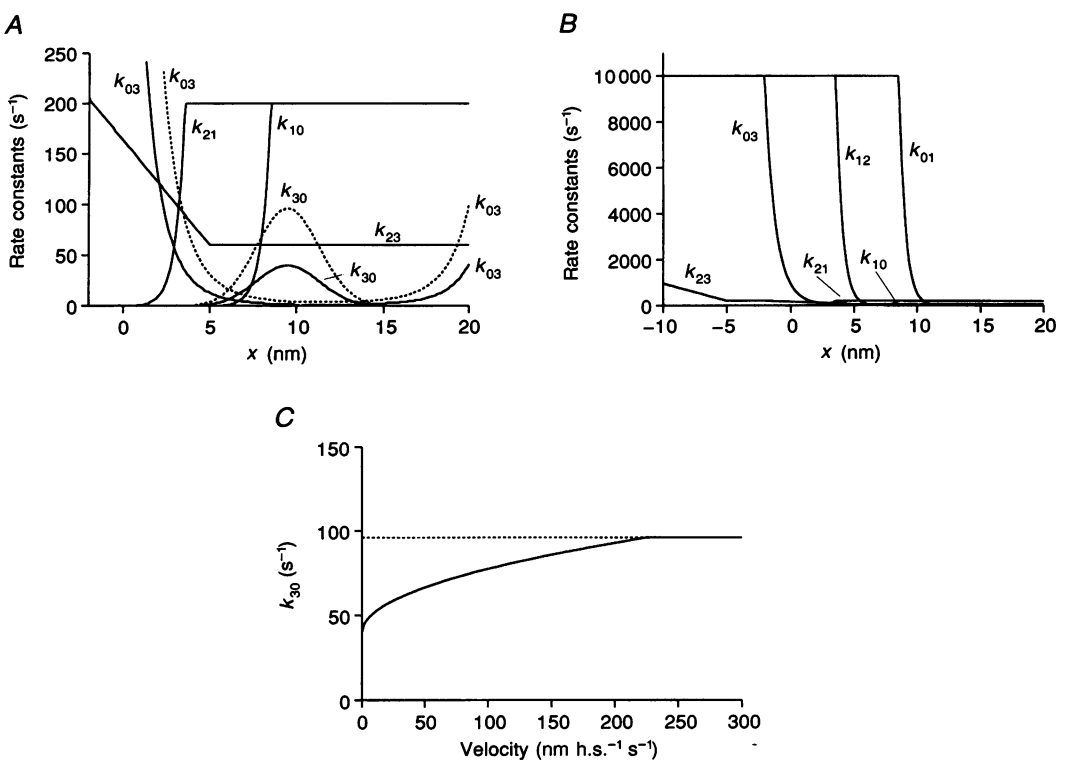

Figure 9. Rate constants of the kinetic model

A and *B*, rate constants given as functions of cross-bridge position (x). The dotted lines in *A* show the rate constants $k_{30}(x)$ and $k_{03}(x)$ used for simulating all data points in Fig. 6*A* and data points at velocities > 225 nm h.s.$^{-1}$ s^{-1} in Fig. 6*B–E*. The continuous lines k_{30} and k_{03} show the numerical values of these rate constants used for simulating isometric contraction in Fig. 6*B–E*. *C*, velocity dependence of rate constant $k_{30}(x,v)$ used in Fig. 6*B–E*. The ordinate refers to the maximum value of the Gaussian x dependence of $k_{30}(x,v)$. Rate constant $k_{03}(x,v)$ was derived from eqn (A1) at all velocities considered.

the time course of the fast tension transients the T_1 and T_2 curves described by Huxley & Simmons (1971). The model is furthermore consistent with the effect of dantrolene on the force–velocity relationship, if it is assumed that dantrolene, by decreasing the intracellular Ca^{2+} concentration, mainly reduces the number of available binding sites on the thin filament (see earlier). This would lead to a shift of the force–velocity relationship to lower force values without any marked change in shape of the force–velocity curve in accordance with the experimental findings. The greater potential of the present model to simulate the force–velocity relationship is attributable to the following features of the model: (1) the existence of a Gaussian x dependence of the attachment rate constant (see below); this implies that there is a region early during the power stroke where cross-bridge attachment is slow; (2) the existence of a force-producing cross-bridge state at the end of the power stroke that is only slightly occupied under isometric conditions and during shortening at low velocity (< approximately 25 nm h.s.$^{-1}$ s^{-1}) but becomes significantly populated during shortening at intermediate and high velocities.

The existence of a region of slow cross-bridge attachment in the beginning of the power stroke leads to a marked reduction in the number of attached cross-bridges, and therefore to a fairly large drop in force, as the speed of shortening is increased within the range 0·05 ('isometric') to 25 nm h.s.$^{-1}$ s^{-1}. This corresponds to the flat region of the force–velocity relationship at force levels greater than $0{\cdot}85P_0$. The decrease in the number of bridges in state A_0 during low-speed shortening mainly involves bridges of high strain (see Results). The force is therefore reduced proportionately more than is the number of attached cross-bridges within this range of velocities and loads. This accords with the experimental finding that there is a greater reduction of force than of stiffness as the velocity of shortening is increased from 0 to 25 nm h.s.$^{-1}$ s^{-1} (Fig. 3*A*, also see Fig. 4*A*).

The region of slow cross-bridge attachment in the beginning of the power stroke is a direct consequence of the fact that the attachment rate constant in our model ($k_{30}(x)$ or $k_{30}(x,v)$) is assumed to have a Gaussian x dependence (Fig. 9*A*). This assumption seems reasonable (see Hill, 1974) and has indeed

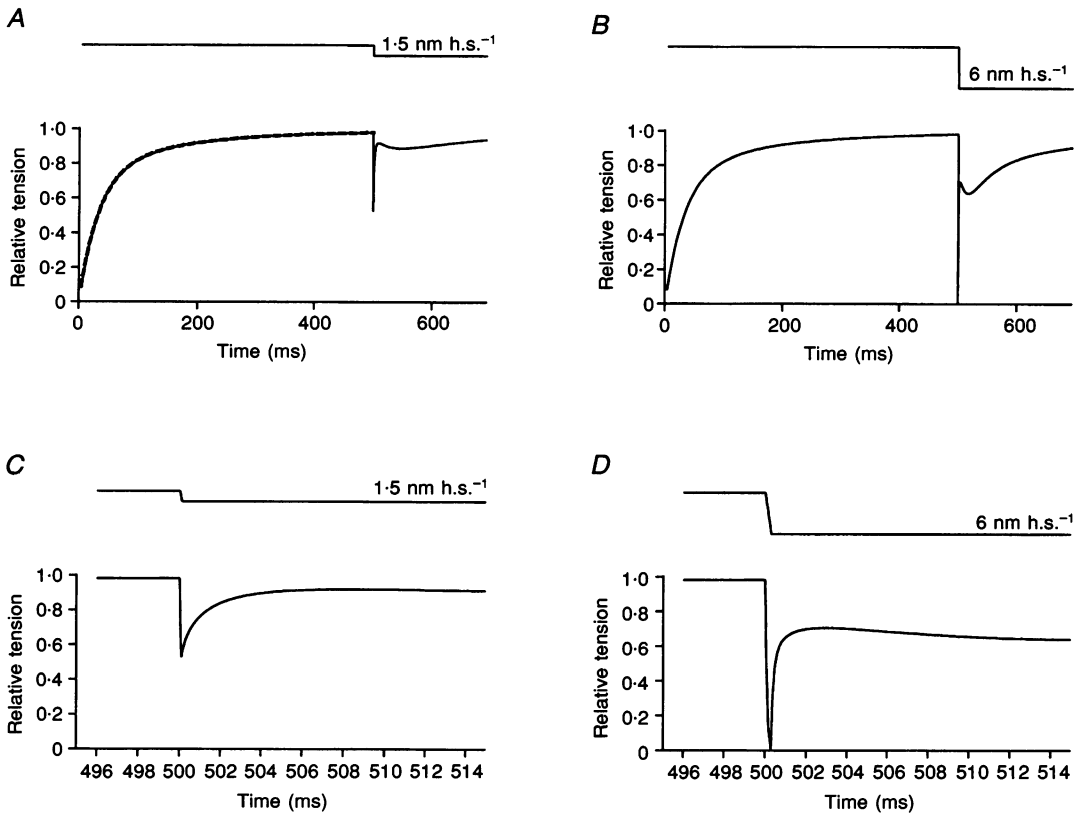

Figure 10. Simulation of the rising phase of fused tetanus and of the tension response to fast length steps during the tetanus plateau

Upper trace in each panel shows the simulated release step. Lower trace shows the simulated force. Releases in *A* and *B* (1·5 and 6 nm h.s.$^{-1}$, respectively) are shown on faster time base in *C* and *D*. The superimposed dashed line in *A* represents a double exponential function fitted by non-linear regression to the simulated data within the interval 5–500 ms: Force $= A(1 - \exp(-\alpha t)) + B(1 - \exp(-\beta t))$. $A = 0{\cdot}74$, $B = 0{\cdot}25$, $\alpha = 30$ s^{-1} and $\beta = 6$ s^{-1}. Corresponding parameters after fitting the equation to experimental records from six intact single muscle fibres were as follows (± S.E.M.): $A = 0{\cdot}83 \pm 0{\cdot}03$, $B = 0{\cdot}17 \pm 0{\cdot}03$, $\alpha = 23 \pm 2$ s^{-1} and $\beta = 6 \pm 1$ s^{-1}.

been adopted before (e.g. Eisenberg *et al.* 1980). It is noteworthy, however, that in the model of Eisenberg and co-workers the equivalent attachment step did not limit the cycling rate of the bridges during shortening, and the Gaussian x dependence of the attachment rate constant therefore had no influence on the shape of the force–velocity curve in the high-force range in their case. The assumption that the attachment rate constant is low in a fraction of the bridges is in line with the observation that the rising phase of a tetanus cannot be fitted faithfully by a single exponential function (Ford, Huxley & Simmons, 1986). A double exponential, on the other hand, provides a very good fit to the tension rise during tetanus. This applies both to recordings from intact muscle fibres and to tetani simulated by the present model (see Fig. 10, Appendix).

The existence of a cross-bridge state at the end of the working cycle (A_2 in our model) that has few attached bridges during isometric activity but becomes greatly populated during shortening has been proposed earlier. Such a cross-bridge state was thus included in the models of Lombardi & Piazzesi (1990) and Piazzesi, Francini, Linari & Lombardi (1992) which were developed to account for various mechanical properties of the muscle during isometric tetani and during stretch ramps in tetanic contractions. The relatively small number of attached cross-bridges in A_2 during isometric activity is largely due to the low numerical value of $k_{12}(x)$ within the 'isometric' working range. This leads to a low average cycling rate (0·25 s^{-1}) in the model consistent with the low ATP splitting rate during isometric contraction of frog muscle (~1 s^{-1}; Curtin, Gilbert, Kretzschmar & Wilkie, 1974; Homsher, 1987).

The present model includes a velocity dependence of the attachment rate constant $k_{30}(x,v)$, the maximum value of which is assumed to decrease from 96 s^{-1} at velocities of active shortening greater than 225 nm h.s.$^{-1}$ s^{-1} to 40 s^{-1} during isometric activity. It should be pointed out that this feature of the model is not essential for simulating the biphasic shape of the force–velocity relationship, as is demonstrated in Fig. 6*A*. It is required in the model, however, in order to faithfully reproduce the time course of the isometric tetanus and the slow phases (phases 3 and 4 in the analysis of Huxley & Simmons, 1971) of the isometric transient after a fast length step. The variation of $k_{30}(x,v)$ with the speed of shortening is in harmony with several recent findings that point to a different cross-bridge behaviour during shortening and during isometric activity (e.g. Yanagida, Arata & Oosawa, 1985; Lombardi, Piazzesi & Linari, 1992; Higuchi & Goldman, 1995). For example, evidence has been presented to show that the rate of repriming of the cross-bridge power stroke after a release is much greater than the cross-bridge attachment rate during isometric contraction (Lombardi *et al.* 1992). A similar rapid repriming of the power stroke might also be expected to occur during continuous shortening (cf. Piazzesi & Lombardi, 1995). It is also worth pointing out in this connection that the maximum association rate constant found suitable in several previous models for simulating the power output is considerably larger (by a factor of 2 or more) than that required to fit the rising phase of an isometric tetanus (e.g. Huxley, 1957; Cooke, White & Pate, 1994; Piazzesi & Lombardi, 1995).

A point of uncertainty concerns the axial spacing of successive binding sites along the thin filament accessible for a given myosin bridge (see also Discussion in Huxley & Tideswell, 1996). In the present study only one actin site, spaced at 37 nm intervals, is assumed to be within reach of the myosin bridge during shortening and isometric activity. Piazzesi & Lombardi (1995), on the other hand, made the assumption that bridges during shortening are able to detach and thereafter rapidly attach again to an adjacent actin binding site 5 nm apart. Their model accounts, in a straightforward way, for the rapid repriming of the power stroke and predicts that attachment of the cross-bridge to actin may occur at a higher rate during shortening than during isometric contraction. This is in line with the apparent velocity dependence of the attachment rate constant assumed here. However, the model of Piazzesi & Lombardi (1995), while very successful in some respects, does not seem to correctly predict the biphasic shape of the force–velocity and stiffness–velocity relationships in striated muscle. A synthesis of the central ideas of the present model (points 1 and 2 above) and the hypothesis of more closely spaced and readily available binding sites in the model of Piazzesi & Lombardi (1995) may be useful in future attempts to obtain a more complete model of muscle mechanics.

Physiological aspects of the biphasic force–velocity relationship

The biphasic shape of the force–velocity relationship has important implications for the function of the muscle in the body. With this particular design the force–velocity relationship provides relatively high velocities at intermediate loads thus enabling a high maximum power output of the muscle. At the same time, by virtue of the high-force curvature, the muscle has acquired a mechanism that confers mechanical stability on the myofilament system.

The high-force curvature brings the force–velocity relationship into an almost flat region as the load approaches P_0. The flat region extends to approximately 1·6P_0 during stretching at which point any further increase in load leads to a rapid elongation of the muscle (see Fig. 7 in Edman, 1988). Between 90 and 120% of P_0 the velocity of shortening or elongation differs by merely 1–2% of V_{max} (Edman, 1988). That is, the muscle stays nearly isometric within this range and any tendency towards redistribution of sarcomere length between weaker and stronger segments along the muscle fibres is therefore minimized under these conditions. The relatively large differences in contractile strength (~4% of P_0) that may exist along the length of a muscle fibre (Edman, Reggiani & teKronnie, 1985) are therefore partly neutralized in this way.

The flat portion of the force–velocity relationship is of particular significance in situations when the muscle is momentarily overloaded, i.e. when the load on the muscle temporarily exceeds P_0. This may occur, for example, when the leg muscles have to absorb the momentum of the body during jumping and running. Under such conditions, as indicated by the force–velocity relationship, the active muscle fibres will be able to hold the extra load (within the limits given above) with very little change in length. It is difficult to conceive of an extramuscular mechanism that would be equally effective in protecting the muscle from being overstretched. Recruitment of additional motor units in order to match the overload would, for example, not be fast enough to serve the purpose; the muscle would yield and elongate well before any new motor units would come into action. The flat region of the force–velocity relationship may thus be said to represent a highly effective intracellular servomechanism that minimizes the redistribution of sarcomere length along the muscle at high loads and, most significantly, that prevents the muscle from being unduly stretched in situations when the load is suddenly raised above the isometric force.

APPENDIX

Description of cross-bridge model

The cross-bridge model used in the present study is based on the assumption (Huxley & Simmons, 1971) that force is generated by an attached cross-bridge according to a multi-step process in which each new step leads to tighter binding between the actin and myosin moieties. In the present scheme, similar to the models described by Piazzesi & Lombardi (1995) and Huxley & Tideswell (1996), the bridge, after attachment, is assumed to undergo two steps and by each of these steps the linear cross-bridge elasticity is extended by 5 nm. The model thus consists of three attached cross-bridge states denoted A_0, A_1 and A_2 in the scheme presented in Fig. 5. In addition to these states, in which cross-bridges can exist at different degrees of elastic extension or compression, there is one detached cross-bridge state, A_3. Of the three attached states, A_0 represents the weakest binding to actin and A_2 the strongest binding as is illustrated by the free energy diagram in Fig. 8.

The rate constants for the transition between the different cross-bridge states depend on the distance between the bridge and the actin binding site. The distance is expressed in terms of the variable x. This variable is taken as zero when the relative position between a cross-bridge and the nearest actin site is such that the cross-bridge produces zero force if attached in state A_2. The x value is taken as positive when the cross-bridge in this state produces force in the shortening direction. The rate constants in Fig. 5 are illustrated in Fig. 9 as functions of x. In the simulations shown in Fig. 6*B–E* the rate constants k_{30} and k_{03} are assumed to depend on the speed of shortening as well and are referred to as $k_{30}(x,v)$ and $k_{03}(x,v)$. However, in the general description of the model that follows below (also covering simulations in which k_{30} and k_{03} are assumed to be velocity independent, see Fig. 6*A*) the designations $k_{30}(x)$ and $k_{03}(x)$ are used throughout. Except for some simplifying approximations (see below) all forward ($k_{ij}(x)$) and reverse ($k_{ji}(x)$) rate constants in a pair are, for a given x value, related according to the equation:

$$k_{ij}(x)/k_{ji}(x) = \exp(-(G_j(x) - G_i(x))/kT),$$
$$(i,j) \in \{(0,1); (1,2); (3,0)\}. \quad \text{(A1)}$$

In this expression $G_i(x)$ and $G_j(x)$ are the Gibbs free energies of cross-bridges in states A_i and A_j, respectively, at a given x value. T is the absolute temperature (276 K used in the present analysis) and k is the Boltzmann constant. For some rate constants eqn (A1) was not obeyed exactly but some approximations were made. The rate constant $k_{32}(x)$ was thus set to zero for all x values. This was justified since the drop in free energy in the model between the states A_2 and A_3 is large enough to make the detachment step essentially irreversible ($k_{32}/k_{23} < 0{\cdot}0004$ according to eqn (A1)). The following approximations were made in the calculations described in the section 'Simulation of isometric tetanus and of tension transients' below: with the exception of $k_{12}(x)$, any rate constant that was smaller than $0{\cdot}01\ s^{-1}$ in a region was set to zero if the ratio between this constant and the rate constant in the reverse direction was less than 0·0001. The numerical value of $k_{12}(x)$ was not in any case smaller than $0{\cdot}01\ s^{-1}$.

The distance between consecutive binding sites on the thin filament is assumed in the model to be 37 nm which is equal to the distance between two successive cross-overs between the two right-handed helical strands of actin. The large distance between consecutive actin sites means that a cross-bridge detaching from actin is not immediately available for reattachment to a new actin site. A given bridge in the model is thus within reach of only one actin site. However, when a large number of cross-bridges is considered, the distribution in x, i.e. the distribution of the actin sites relative to their nearest myosin head, may be regarded uniform (Huxley, 1957; Hill, 1974). Considering the ensemble of myosin heads in a half-sarcomere of a fibre it may thus be assumed (Huxley, 1957; Hill, 1974) that an equal number of actin binding sites exists for each x value, i.e. between x and dx where dx is infinitesimally small. Therefore, if the probability of a cross-bridge of being in any of the states A_0, A_1, A_2 and A_3 in the interval (x, $x + dx$) is denoted by $a_0(x)$, $a_1(x)$, $a_2(x)$ and $a_3(x)$, respectively, then the sum:

$$\sum_{i=0}^{3} a_i(x) = 1,$$

for all intervals (x, $x + dx$).

The behaviour of the model may be described by the following set of equations in the state probabilities:

$$\frac{da_0}{dt}=\frac{\partial a_0}{\partial x}\frac{dx}{dt}+\frac{\partial a_0}{\partial t}=k_{30}(x)a_3+k_{10}(x)a_1-(k_{03}(x)+k_{01}(x))a_0, \quad \text{(A2)}$$

$$\frac{da_1}{dt}=\frac{\partial a_1}{\partial x}\frac{dx}{dt}+\frac{\partial a_1}{\partial t}=k_{01}(x)a_0+k_{21}(x)a_2-(k_{10}(x)+k_{12}(x))a_1, \quad \text{(A3)}$$

$$\frac{da_2}{dt}=\frac{\partial a_2}{\partial x}\frac{dx}{dt}+\frac{\partial a_2}{\partial t}=k_{12}(x)a_1+k_{32}(x)a_3-(k_{21}(x)+k_{23}(x))a_2, \quad \text{(A4)}$$

$$\frac{da_3}{dt}=\frac{\partial a_3}{\partial x}\frac{dx}{dt}+\frac{\partial a_3}{\partial t}=k_{23}(x)a_2+k_{03}(x)a_0-(k_{32}(x)+k_{30}(x))a_3, \quad \text{(A5)}$$

$$\sum_{i=0}^{3}a_i(x,t)=1, \qquad \text{for all } (x,\ x+dx) \text{ and } t. \quad \text{(A6)}$$

In eqns (A2)–(A5) $a_i \equiv a_i(x,t)$; $i = 0,1,2,3$ but the arguments have been omitted above for practical reasons.

Average force, $\langle F \rangle$, per myosin head may be obtained from the relationship:

$$\langle F \rangle = \frac{K}{\delta}\int_{-\delta/2}^{\delta/2}[a_0(x)(x-10)+a_1(x)(x-5)+a_2(x)x]dx, \quad \text{(A7)}$$

where K is the cross-bridge stiffness ($0{\cdot}4$ kT nm$^{-2} \approx 1{\cdot}5$ pN nm^{-1}) and δ is the distance between adjacent actin sites (37 nm). The variable x is given in nanometres.

The average stiffness, $\langle S \rangle$ was obtained from the relationship:

$$\langle S \rangle = \frac{K}{\delta}\int_{-\delta/2}^{\delta/2}[a_0(x)+a_1(x)+a_2(x)]dx. \quad \text{(A8)}$$

Implementation of the model

Simulation of steady-state force–velocity data. During steady-state shortening the partial derivatives $\partial a_i(x,t)/\partial t$ ($i = 0,1,2,3$) in eqns (A2)–(A5) are equal to zero and the shortening velocity ($v = dx/dt < 0$) is constant. The set of eqns (A2)–(A6) can therefore, under these conditions, be solved as a system of ordinary differential equations in x with x-dependent rate constants. Such solutions were obtained for relevant x values and for velocities varying between $v = 0{\cdot}05$ nm s^{-1} and $v = 1660$ nm s^{-1}. The solutions were obtained by means of a fourth order Runge-Kutta method with automatic step size adjustment. Varying the error tolerance level in the algorithms by a factor of 100 did not significantly affect the outcome of the calculation. The algorithms were carried out in the commercially available program Simnon (SSPA Systems, Gothenburg, Sweden).

Simulation of isometric tetanus and of tension transients. Although the main purpose of the model in the present study was to simulate the force–stiffness–velocity relationships described earlier (see Results), it was also of interest to test the validity of the model for simulating the time course of the isometric tetanus and the tension transients in response to fast length steps. To this end the model was implemented in Pascal code using Turbo Pascal software. Differential equations were solved numerically using an implicit Runge-Kutta method (second order) based on the trapezoidal rule (cf. Gear, 1971). This method is suitable for the stiff differential equations of the present work. Solutions of the set of eqns (A2)–(A6) were obtained for 351 equally spaced x values (x_j) in the range $-10 \text{ nm} \leqslant x_j \leqslant 25$ nm ($j = 1,2,\ldots 351$; $x_1 = -10$ nm, $x_{351} = 25$ nm). The boundary conditions for the state probabilities were (for all values of the time, t):

$$a_i(-10,t) = a_i(25,t) = 0, \qquad i = 0, 1, 2,$$

$$a_3(-10,t) = a_3(25,t) = 1.$$

The solution of the differential equations for a given value x_j provides an average value for the range:

$$x_j - \Delta x/2 \leqslant x < x_j + \Delta x/2,$$

where the distance Δx between adjacent x_j values is $0{\cdot}1$ nm. Reducing Δx by 50% did not produce any significant change of the computed behaviour of the model.

In the following $a_0(x_j)$, $a_1(x_j)$, $a_2(x_j)$ and $a_3(x_j)$ represent the probability that bridges in the range:

$$x_j - \Delta x/2 \leqslant x < x_j + \Delta x/2,$$

are in the states A_0, A_1, A_2 and A_3, respectively. The average force and stiffness were determined from eqns (A7)–(A8) using the trapezoidal rule to calculate the integrals. The simulations were started with the initial condition where $a_3(x_j) = 1$ and $a_0(x_j) = a_1(x_j) = a_2(x_j) = 0$ for all values of j. This would correspond to the relaxed state in a muscle fibre with all cross-bridges being detached from actin. After starting the simulation in this condition there was first a rise in force corresponding to the events recorded during the onset of an isometric tetanus. In simulating the rising phase and the tetanus plateau the time step (Δt) for the numerical solution of the differential equations was normally $0{\cdot}8$ ms. The results of the simulations were not significantly affected by a twofold change of this value. As illustrated in Fig. 10*A*, the rising phase of an isometric tetanus predicted by the model agrees well with recordings from intact fibres at the temperature (1–3 °C) considered.

Tension transients in response to fast release steps were simulated when the isometric force was $> 98\%$ of the steady-state value (simulated time $\geqslant 500$ ms). Fast releases with a finite velocity (length step complete in 100–600 μs depending on the amplitude of the length change) were approximated in the simulations by n times ($5 \leqslant n \leqslant 30$) shifting of the cross-bridge population (for each xj value) by a number of discrete j values equal to $(\Delta L/n)/\Delta x$. Here ΔL is the total amplitude of release, the numerical value of ΔL and n being chosen to make the ratio $(\Delta L/n)/\Delta x$ an integer in each case. By using several consecutive substeps to

simulate the entire length change a finite velocity of the complete release movement was obtained. In this way large negative tensions during the release were prevented thus simulating the true experimental situation more faithfully.

After each substep (amplitude $\Delta L/n$) a time interval of 20 μs was allowed for a new distribution of cross-bridges to be established before the next substep was initiated. This new cross-bridge population was calculated by numerical solution of eqns (A2)–(A6) using the appropriate state probabilities $a_i(x_j)$ ($i = 0,1,2,3$; all j) as initial values. The time interval, Δt, used for numerical integration of the differential eqns (A2)–(A5), was 4 μs. The procedure was repeated n times until the total release movement, ΔL, had been completed. No further shifts of the cross-bridge population along the x-axis were thereafter imposed in the simulation, but the numerical solution of eqns (A2)–(A6) was continued in order to determine the force recovery after the release. During the first millisecond after the release Δt was 4 μs. This value was increased to 10 μs in the interval 1–5 ms after the release, to 60 μs between 5 and 40 ms, to 100 μs between 40 and 250 ms after the release and to 200 μs for the remainder of the simulation period. A doubling of these values of Δt did not significantly change the outcome of the simulation.

Figure 10 shows simulated tension transients in response to two different release steps performed during the plateau of the isometric tetanus. The tension response can be seen to exhibit the same general features as observed in muscle fibres with distinct T_1 and T_2 components and a final slow recovery of force towards the pre-release level. Plottings of T_1 and T_2 curves (not illustrated) likewise agree well with measurements on intact fibres (Ford, Huxley & Simmons, 1977; Piazzesi *et al.* 1992), the curves extrapolating to the x-axis at 3 and 10 nm, respectively.

Bagni, M. A., Cecchi, G., Colomo, F. & Poggesi, C. (1990). Tension and stiffness of frog muscle fibres at full filament overlap. *Journal of Muscle Research and Cell Motility* **11**, 371–377.

Cooke, R., White, H. & Pate, E. (1994). A model of the release of myosin heads from actin in rapidly contracting muscle fibers. *Biophysical Journal* **66**, 778–788.

Curtin, N. A. & Edman, K. A. P. (1994). Force–velocity relation for frog muscle fibres: effects of moderate fatigue and of intracellular acidification. *Journal of Physiology* **475**, 483–494.

Curtin, N. A., Gilbert, C., Kretzschmar, K. M. & Wilkie, D. R. (1974). The effect of the performance of work on total energy output and metabolism during muscular contraction. *Journal of Physiology* **238**, 455–472.

Danko, S., Kim, D. H., Sreter, F. A. & Ikemoto, N. (1985). Inhibitors of Ca^{2+} release from the isolated sarcoplasmic reticulum. II. The effects of dantrolene on Ca^{2+} release induced by caffeine, Ca^{2+} and depolarization. *Biochimica et Biophysica Acta* **816**, 18–24.

Desmedt, J. E. & Hainaut, K. (1977). Inhibition of the intracellular release of calcium by dantrolene in barnacle giant muscle fibres. *Journal of Physiology* **265**, 565–585.

Edman, K. A. P. (1979). The velocity of unloaded shortening and its relation to sarcomere length and isometric force in vertebrate muscle fibres. *Journal of Physiology* **291**, 143–159.

Edman, K. A. P. (1988). Double-hyperbolic force–velocity relation in frog muscle fibres. *Journal of Physiology* **404**, 301–321.

Edman, K. A. P. (1993). Mechanism underlying double-hyperbolic force–velocity relation in vertebrate skeletal muscle. In *Mechanism of Myofilament Sliding in Muscle Contraction*, ed. Sugi, H. & Pollack, G. H., pp. 667–678. Plenum Press, New York.

Edman, K. A. P. & Caputo, C. (1993). High-force curvature of the force–velocity relation studied in isolated muscle fibers of the frog. *Biophysical Journal* **64**, A250.

Edman, K. A. P. & Lou, F. (1990). Changes in force and stiffness induced by fatigue and intracellular acidification in frog muscle fibres. *Journal of Physiology* **424**, 133–149.

Edman, K. A. P., Mulieri, L. A. & Scubon-Mulieri, B. (1976). Non-hyperbolic force-velocity relationship in single muscle fibres. *Acta Physiologica Scandinavica* **98**, 143–156.

Edman, K. A. P. & Reggiani, C. (1984). Redistribution of sarcomere length during isometric contraction of frog muscle fibres and its relation to tension creep. *Journal of Physiology* **351**, 169–198.

Edman, K. A. P. & Reggiani, C. (1987). The sarcomere length–tension relation determined in short segments of intact muscle fibres of the frog. *Journal of Physiology* **385**, 709–732.

Edman, K. A. P., Reggiani, C. & teKronnie, G. (1985). Differences in maximum velocity of shortening along single muscle fibres of the frog. *Journal of Physiology* **365**, 147–163.

Eisenberg, E. & Hill, T. L. (1978). A cross-bridge model of muscle contraction. *Progress in Biophysics and Molecular Biology* **33**, 55–82.

Eisenberg, E., Hill, T. L. & Chen, Y. (1980). Cross-bridge model of muscle contraction. Quantitative analysis. *Biophysical Journal* **29**, 195–227.

Fenn, W. O. & Marsh, B. S. (1935). Muscular force at different speeds of shortening. *Journal of Physiology* **85**, 277–297.

Ford, L. E., Huxley, A. F. & Simmons, R. M. (1977). Tension responses to sudden length change in stimulated frog muscle fibres near slack length. *Journal of Physiology* **269**, 441–515.

Ford, L. E., Huxley, A. F. & Simmons, R. M. (1986). Tension transients during the rise of tetanic tension in frog muscle fibres. *Journal of Physiology* **372**, 595–609.

Gear, C. W. (1971). *Numerical Initial Value Problems in Ordinary Differential Equations*. Prentice-Hall, Englewood Cliffs, NJ, USA.

Higuchi, H. & Goldman, Y. E. (1995). Sliding distance per ATP molecule hydrolyzed by myosin heads during isotonic shortening of skinned muscle fibers. *Biophysical Journal* **69**, 1491–1507.

Higuchi, H., Yanagida, T. & Goldman, Y. (1995). Compliance of thin filaments in skinned fibers of rabbit skeletal muscle. *Biophysical Journal* **69**, 1000–1010.

Hill, A. V. (1938). The heat of shortening and the dynamic constants of muscle. *Proceedings of the Royal Society* B **126**, 136–195.

Hill, T. L. (1974). Theoretical formalism for the sliding filament model of contraction of striated muscle. Part I. *Progress in Biophysics and Molecular Biology* **28**, 267–340.

Homsher, E. (1987). Muscle enthalpy production and its relationship to actomyosin ATPase. *Annual Review of Physiology* **49**, 673–690.

Huxley, A. F. (1957). Muscle structure and theories of contraction. *Progress in Biophysics and Biophysical Chemistry* **7**, 255–318.

Huxley, A. F. & Simmons, R. M. (1971). Proposed mechanism of force generation in striated muscle. *Nature* **233**, 533–538.

HUXLEY, A. F. & TIDESWELL, S. (1996). Filament compliance and tension transients in muscle. *Journal of Muscle Research and Cell Motility* **17**, 507–511.

HUXLEY, H. E., STEWART, A., SOSA, H. & IRVING, T. (1994). X-ray diffraction measurements of the extensibility of actin and myosin filaments in contracting muscle. *Biophysical Journal* **67**, 2411–2421.

KOJIMA, H., ISHIJIMA, A. & YANAGIDA, T. (1994). Direct measurement of stiffness of single actin filaments with and without tropomyosin by an *in vitro* nanomanipulation. *Proceedings of the National Academy of Sciences of the USA* **91**, 12962–12966.

LOMBARDI, V. & PIAZZESI, G. (1990). The contractile response during steady lengthening of stimulated frog muscle fibres. *Journal of Physiology* **431**, 141–171.

LOMBARDI, V., PIAZZESI, G. & LINARI, M. (1992). Rapid regeneration of the actin–myosin power stroke in contracting muscle. *Nature* **355**, 638–641.

LOU, F. & SUN, Y.-B. (1993). The high-force region of the force-velocity relation in frog skinned muscle fibres. *Acta Physiologica Scandinavica* **148**, 243–252.

PIAZZESI, G., FRANCINI, F., LINARI, M. & LOMBARDI, V. (1992). Tension transients during steady lengthening of tetanized muscle fibres of the frog. *Journal of Physiology* **445**, 659–711.

PIAZZESI, G. & LOMBARDI, V. (1995). A cross-bridge model that is able to explain mechanical and energetic properties of shortening muscle. *Biophysical Journal* **68**, 1966–1979.

SUN, Y.-B., LOU, F. & EDMAN, K. A. P. (1995). The effects of 2,3-butanedione monoxime (BDM) on the force–velocity relation in single muscle fibres of the frog. *Acta Physiologica Scandinavica* **153**, 325–334.

VAN WINKLE, W. B. (1976). Calcium release from skeletal muscle sarcoplasmic reticulum: site of action of dantrolene sodium. *Science* **193**, 1130–1131.

WAKABAYASHI, K., SUGIMOTO, Y., TANAKA, H., UENO, Y., TAKEZAWA, Y. & AMEMIYA, Y. (1994). X-ray diffraction evidence for the extensibility of actin and myosin filaments during muscle contraction. *Biophysical Journal* **67**, 2422–2435.

WOLEDGE, R. C., CURTIN, N. A. & HOMSHER, E. (1985). *Energetic Aspects of Muscle Contraction.* Academic Press, London.

YANAGIDA, T., ARATA, T. & OOSAWA, F. (1985). Sliding distance of actin filament induced by a myosin cross-bridge during one ATP hydrolysis cycle. *Nature* **316**, 366–369.

Acknowledgements

This work was supported by grants from the Swedish Medical Research Council (14X-184) and the Medical Faculty, University of Lund. C.C. was supported by a Visiting Scientist Fellowship (K89-14V-08899-01) from the Swedish Medical Research Council.

Author's present address

C. Caputo: Centro de Biophísica y Bioquímica, Instituto Venezolano de Investigaciones Cinetificas, Apartado 21827, Caracas 1020-A, Venezuela.

Author's email address

K. A. P. Edman: paul.edman@farm.lu.se

Received 4 February 1997; accepted 8 May 1997.